The Astrophysical Journal Letters, 776:L41 (6pp), 2013 October 20 doi:10.1088/2041-8205/776/2/L41

A DIRECT MEASUREMENT OF THE LINEAR BIAS OF MID-INFRARED-SELECTED QUASARS AT $z \approx 1$ USING COSMIC MICROWAVE BACKGROUND LENSING

J. E. Geach[1,2], R. C. Hickox[3], L. E. Bleem[4,5,6], M. Brodwin[7], G. P. Holder[2], K. A. Aird[8], B. A. Benson[4,9], S. Bhattacharya[4,6], J. E. Carlstrom[4,5,6,9,10], C. L. Chang[4,6,9], H.-M. Cho[11], T. M. Crawford[4,10], A. T. Crites[4,10], T. de Haan[2], M. A. Dobbs[2], J. Dudley[2], E. M. George[12], K. N. Hainline[3], N. W. Halverson[13], W. L. Holzapfel[12], S. Hoover[4,5], Z. Hou[14], J. D. Hrubes[8], R. Keisler[4,5], L. Knox[14], A. T. Lee[12,15], E. M. Leitch[4,10], M. Lueker[16], D. Luong-Van[8], D. P. Marrone[17], J. J. McMahon[18], J. Mehl[4,6], S. S. Meyer[4,5,9,10], M. Millea[14], J. J. Mohr[19,20,21], T. E. Montroy[22], A. D. Myers[23], S. Padin[4,10,16], T. Plagge[4,10], C. Pryke[24], C. L. Reichardt[12], J. E. Ruhl[22], J. T. Sayre[22], K. K. Schaffer[4,9,25], L. Shaw[2], E. Shirokoff[12], H. G. Spieler[15], Z. Staniszewski[22], A. A. Stark[26], K. T. Story[4,5], A. van Engelen[2], K. Vanderlinde[2,27,28], J. D. Vieira[16], R. Williamson[4,10], and O. Zahn[29]

[1] Centre for Astrophysics Research, Science & Technology Research Institute, University of Hertfordshire, Hatfield, AL10 9AB, UK; j.geach@herts.ac.uk
[2] Department of Physics, McGill University, Montreal, Quebec H3A 2T8, Canada
[3] Department of Physics and Astronomy, Dartmouth College, 6127 Wilder Laboratory, Hanover, NH 03755, USA
[4] Kavli Institute for Cosmological Physics, University of Chicago, Chicago, IL 60637, USA
[5] Department of Physics, University of Chicago, Chicago, IL 60637, USA
[6] High Energy Physics Division, Argonne National Laboratory, Argonne, IL 60440, USA
[7] Department of Physics and Astronomy, University of Missouri, Kansas City, MO 64110, USA
[8] University of Chicago, Chicago, IL 60637, USA
[9] Enrico Fermi Institute, University of Chicago, Chicago, IL 60637, USA
[10] Department of Astronomy and Astrophysics, University of Chicago, Chicago, IL 60637, USA
[11] NIST Quantum Devices Group, Boulder, CO 80305, USA
[12] Department of Physics, University of California, Berkeley, CA 94720, USA
[13] Department of Astrophysical and Planetary Sciences and Department of Physics, University of Colorado, Boulder, CO 80309, USA
[14] Department of Physics, University of California, Davis, CA 95616, USA
[15] Physics Division, Lawrence Berkeley National Laboratory, Berkeley, CA 94720, USA
[16] California Institute of Technology, Pasadena, CA 91125, USA
[17] Steward Observatory, University of Arizona, Tucson, AZ 85721, USA
[18] Department of Physics, University of Michigan, Ann Arbor, MI 48109, USA
[19] Department of Physics, Ludwig-Maximilians-Universität, D-81679 München, Germany
[20] Excellence Cluster Universe, D-85748 Garching, Germany
[21] Max-Planck-Institut für extraterrestrische Physik, D-85748 Garching, Germany
[22] Physics Department, Center for Education and Research in Cosmology and Astrophysics, Case Western Reserve University, Cleveland, OH 44106, USA
[23] Department of Physics and Astronomy, University of Wyoming, Laramie, WY 82072, USA
[24] Department of Physics, University of Minnesota, Minneapolis, MN 55455, USA
[25] Liberal Arts Department, School of the Art Institute of Chicago, Chicago, IL 60603, USA
[26] Harvard-Smithsonian Center for Astrophysics, Cambridge, MA 02138, USA
[27] Dunlap Institute for Astronomy and Astrophysics, University of Toronto, 50 St George St, Toronto, ON M5S 3H4, Canada
[28] Department of Astronomy and Astrophysics, University of Toronto, 50 St George St, Toronto, ON M5S 3H4, Canada
[29] Berkeley Center for Cosmological Physics, Department of Physics, University of California, Berkeley, CA 94720, USA
Received 2013 July 3; accepted 2013 September 20; published 2013 October 7

ABSTRACT

We measure the cross-power spectrum of the projected mass density as traced by the convergence of the cosmic microwave background lensing field from the South Pole Telescope (SPT) and a sample of Type 1 and 2 (unobscured and obscured) quasars at $\langle z \rangle \sim 1$ selected with the *Wide-field Infrared Survey Explorer*, over 2500 deg^2. The cross-power spectrum is detected at $\approx 7\sigma$, and we measure a linear bias $b = 1.61 \pm 0.22$, consistent with clustering analyses. Using an independent lensing map, derived from *Planck* observations, to measure the cross-spectrum, we find excellent agreement with the SPT analysis. The bias of the combined sample of Type 1 and 2 quasars determined in this work is similar to that previously determined for Type 1 quasars alone; we conclude that obscured and unobscured quasars trace the matter field in a similar way. This result has implications for our understanding of quasar unification and evolution schemes.

Key word: cosmology: observations

Online-only material: color figures

1. INTRODUCTION

The trajectories of photons that comprise the cosmic microwave background (CMB) have been gravitationally deflected by large scale structure. The observational consequence is a smoothing of the CMB temperature power spectrum, and the introduction of correlations between what were originally independent modes. These effects allow one to map the total projected gravitational potential of the universe back to the surface of last scattering.

CMB experiments have now achieved the sensitivity and resolution to directly detect the non-Gaussian signature left on the CMB by gravitational lensing (Das et al. 2011; van Engelen et al. 2012; Planck Collaboration XVII 2013a). A method of mapping the lensing potential is the optimal quadratic estimator (Seljak & Zaldarriaga 1999; Hu 2001) that allows one to separate

the lensing perturbation from the intrinsic power spectrum. The redshift where the weight of the lensing kernel peaks is close to the maximum in the global volume-averaged star formation and black hole growth rates; CMB lensing studies therefore promise exciting new insights into the complex relationship between the growth of luminous galaxies and the dark matter overdensities they inhabit, in additional to cosmological applications (Smith et al. 2007; Hirata et al. 2008; Sherwin et al. 2012; Bleem et al. 2012; Holder et al. 2013; Planck Collaboration XVIII 2013b).

Quasars are visible over cosmological distances even in relatively shallow surveys, and have a long history as cosmological probes. They also represent an important phase in the evolution of massive galaxies, since their luminosities arise from an episode of supermassive black hole growth. How this phase dovetails with the global scheme of galaxy evolution remains to be fully understood. Sherwin et al. (2012) presented the first detection of a significant (3.8σ) cross-correlation signal between Sloan Digital Sky Survey (SDSS) optically-selected quasars and the CMB lensing convergence measured by the Atacama Cosmology Telescope over 320 deg^2. Here we use the *Wide-field Infrared Survey Explorer* (*WISE*; Wright et al. 2010) to select both Type 1 and Type 2 (unobscured and obscured) quasars over a 2500 deg^2 field for which we have a map of the CMB measured by the South Pole Telescope (SPT; Carlstrom et al. 2011; Story et al. 2012).

In this Letter, we present a cross-correlation analysis examining the relationship between the combined Type 1 and 2 quasar population and the matter field. A ΛCDM cosmology defined by the parameters measured with the *Wilkinson Microwave Anisotropy Probe* (7 year results including baryonic acoustic oscillation and Hubble constant constraints; Komatsu et al. 2011) is assumed and throughout *WISE* fluxes are quoted on the Vega magnitude system.

2. DATA

2.1. SPT Lensing Convergence Map

The SPT temperature survey (Carlstrom et al. 2011) covers 2500 deg^2 ($\alpha = 20^{\rm hr} \rightarrow 7^{\rm hr}$, $\delta = -65^\circ \rightarrow -40^\circ$) at $\nu_{\rm obs} = 95$, 150, and 220 GHz to typical 1σ depths of 40, 18, and 70 μK-arcmin. For this work we only use 150 GHz data. The full survey comprises many individual fields which are combined for this work to make CMB temperature maps that are 17° on a side. Maps of the gravitational potential (van Engelen et al. 2012) for these 17° fields are mosaicked into a single 2500 deg^2 map at $3'$ resolution. We use a single lensing filter for all regions of the SPT survey; because the noise fluctuates mildly from field to field, this is not optimal. For precise measures of the lensing power spectrum (van Engelen et al. 2012; O. Zahn et al., in preparation) optimal lensing filters are made using the individual noise levels of each of the original 100 deg^2 individual fields.

This procedure is repeated for 40 sets of simulations, which consist of lensed CMB maps and realistic SPT noise, following the procedure outlined in van Engelen et al. (2012). The resulting full-field simulated gravitational lensing maps are cross-correlated with the input maps to obtain an effective transfer function that can be used to correct the observed cross-correlations (Section 4.1). As part of this validation procedure, we also tested the reliability of the "flat sky" approximation. Projecting the input full-sky gravitational potential maps into our Zenithal Equal Area projection, we verified that the mean power spectra of the projected 2500 deg^2 maps agree with the full-sky curved-sky power spectrum to much better than a few per cent for $l > 20$, and that power spectra of 2500 deg^2 flat sky maps agreed to similar precision with curved-sky power spectra.

Any correlation between the CMB foreground power and the galaxy density can lead to a small bias in the CMB lensing-galaxy cross-power on large scales (van Engelen et al. 2012; Bleem et al. 2012). For infrared intensity fluctuations or the thermal Sunyaev–Zel'dovich effect, this was found to be on the order of a few percent (van Engelen et al. 2012), and it is not expected to be substantially larger for quasars.

2.2. WISE Quasar Selection

2.2.1. Selection of Quasars at 3.4–4.6 μm

WISE has mapped the sky at 3.4, 4.6, 12, and 22 μm (*W1–W4*), and offers a unique resource to study the demographics of quasars and active galactic nuclei (AGNs).[30]

We create a catalog of galaxies from the *WISE* All-sky Release,[31] selecting all sources with (1) signal-to-noise in *W2* *w2snr* $\geqslant$ 10, (2) *W2* magnitude *w2mpro* $\leqslant$ 15 mag, (3) data quality flags *cc_flags* = "0" in both the *W1* and *W2* bands, (4) number of point spread function (PSF) components fit *nb* = 1, and (5) number of active deblends *na* = 0. The choice of signal-to-noise (1) and magnitude limit (2) in the *W2* (4.6 μm) band is to ensure approximately uniform completeness across the full SPT footprint. The data quality parameter (3) ensures that contamination of the catalog by false detections and errors in PSF-fit photometry from instrumental artifacts is minimized. We also require that only a single PSF component is fit to measure the photometry (4) and the source has not been actively de-blended (5), improving reliability.

The selection of quasars in the mid-infrared is a well-established technique (Lacy et al. 2004; Stern et al. 2005). Assef et al. (2013) show that in the *WISE* bands a selection of $W1 - W2 \geqslant 0.8$ and $W2 \leqslant 15$ mag returns a reliable sample of both Type 1 and 2 AGN. Figure 1 illustrates the efficacy of this selection in the *W1–W2–W3* color plane, using spectroscopically classified sources selected from the SDSS (Data Release 7; Abazajian et al. 2009), matched to *WISE*. With the *WISE* AGN cut, we select 107,469 objects, corresponding to a surface density of 42 deg^{-2}.

2.2.2. Redshift Distribution

To obtain an estimate of the redshift distribution of our sample, we select objects from the *WISE* All-sky Survey catalog using the criteria described above within the 9 deg^2 Boötes survey field, which has extensive spectroscopy as part of the 7.9 deg^2 AGN and Galaxy Evolution Survey (AGES; Kochanek et al. 2012) and photometric redshift estimates using optical and *Spitzer* IRAC imaging (Brodwin et al. 2006).

Figure 2 shows the redshift distribution of 379 *WISE* sources matching our selection in the AGES survey region with spectroscopic redshifts (89%) or photometric redshift estimates ($\delta z \approx 0.3$). The distribution peaks at $\langle z \rangle = 1.1$ and has a spread of $\Delta z = 0.6$. We have redshift estimates for 93% of the *WISE*-selected AGN in the AGES region, and so this is likely to be a robust model of the redshift distribution of identically-selected sources in the SPT field. Note that the spectroscopic Boötes data allows us to estimate the contamination rate from non-AGN in our selection, which is $\lesssim$15%.

[30] In this work we use the term "quasar" to refer to both classical quasars and AGN since the majority of the objects in our sample have high luminosities characteristic of "quasars."

[31] http://irsa.ipac.caltech.edu/Missions/wise.html

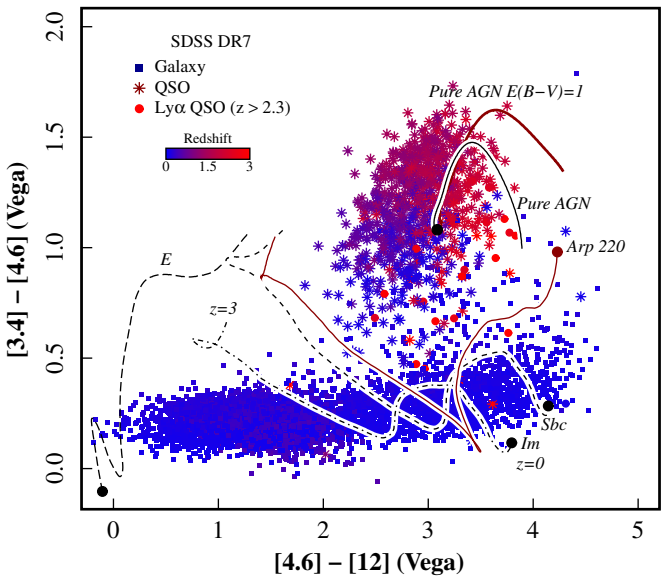

Figure 1. *WISE W1–W2–W3* (3.4–4.6–12 μm) colors of 6000 spectroscopically classified galaxies and quasars from SDSS. Tracks show the colors of typical normal galaxies (elliptical [E], mid-type spiral [Sbc] and irregular/starburst [Im]), a prototypical ultraluminous starburst galaxy (Arp 220) and a zero star formation quasar seen at $0 < z < 3$ (Polletta et al. 2007; Vega et al. 2008; Assef et al. 2013; Yan et al. 2013). We show the effect of internal reddening on the quasar track with an extinction of $E(B-V) = 1$ mag. This demonstrates how *WISE* colors can be used to cleanly separate quasars from normal galaxies.

(A color version of this figure is available in the online journal.)

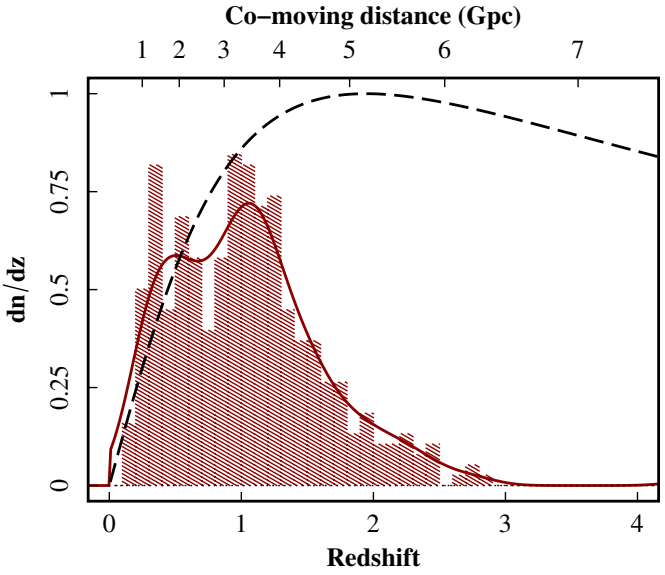

Figure 2. Normalized redshift distribution of 379 quasars selected using the criteria $W1-W2 \geqslant 0.8$ and $W2 \leqslant 15$ mag in the 7.9 deg^2 Boötes/AGES field (Section 2.2.2). The solid line shows the density estimate of the discrete redshift distribution which we use as the model dn/dz. The dashed line shows the shape of the CMB lensing kernel, plotted as $(d\chi/dz)W^\kappa$ (Section 3).

(A color version of this figure is available in the online journal.)

3. CMB LENSING THEORY REVIEW

We briefly review the formalism presented in Bleem et al. (2012). The lensing convergence $\kappa = -\nabla \cdot \mathbf{d}/2$ (where $\mathbf{d}$ is the deflection field) along a line of sight $\hat{\mathbf{n}}$, can be expressed as the integral, over comoving distance χ, of the fractional overdensity of matter $\delta(\mathbf{r}, z)$, multiplied by the lensing kernel, W^κ:

$$\kappa(\hat{\mathbf{n}}) = \int d\chi\, W^\kappa(\chi)\delta(\chi\hat{\mathbf{n}}, z(\chi)), \tag{1}$$

where the lensing kernel is (Cooray & Hu 2000; Song et al. 2003):

$$W^\kappa(\chi) = \frac{3}{2}\Omega_{\rm m}H_0^2\frac{\chi}{a(\chi)}\frac{\chi_{\rm CMB}-\chi}{\chi_{\rm CMB}}. \tag{2}$$

Here $\Omega_{\rm m}$ and H_0 are the present-day values of the ratio of the matter density to the critical density and Hubble parameter respectively, and $a(\chi)$ is the scale factor. The comoving distance to the surface of last scattering $\chi_{\rm CMB} \approx 14$ Gpc in our cosmology.

Quasars, like all galaxies, are biased tracers of the matter field, and so fluctuations in the galaxy density can be expressed

$$g(\hat{\mathbf{n}}) = \int d\chi\, W^g(\chi)\delta(\chi\hat{\mathbf{n}}, z(\chi)) \tag{3}$$

where $W^g(\chi)$ is the quasar distribution kernel

$$W^g(\chi) = \frac{dz}{d\chi}\frac{dn(z)}{dz}b(\chi) \tag{4}$$

where $dn(z)/dz$ is the normalized redshift distribution of the population, and b is the bias. Comparing Equations (2) and (4), the lensing quantity analogous to dn/dz is $(d\chi/dz)W^\kappa$. This is plotted in Figure 2 for comparison. With these defined, the cross-power at angular frequency l, assuming the Limber approximation (Limber 1953; Kaiser 1992), is

$$C_l^{\kappa g} = \int dz\frac{d\chi}{dz}\frac{1}{\chi^2}W^\kappa(\chi)W^g(\chi)P\left(\frac{l}{\chi}, z\right) \tag{5}$$

where $P(k = l/\chi, z)$ is the non-linear matter power spectrum, which we generate from the Code for Anisotropies in the Microwave Background (Lewis et al. 2000, online version[32]) which calculates the non-linear matter power spectrum using HALOFIT (Smith et al. 2003).

4. ANALYSIS AND RESULTS

A quasar density map, expressed as $\delta = (\rho - \langle\rho\rangle)/\langle\rho\rangle$, is generated from the *WISE* catalog on a grid matching the $3'$ pixel^{-1} scale of the convergence map (Figure 3). Both the quasar map and the SPT lensing map have been smoothed to show scales where the lensing convergence map has significant signal-to-noise.

If quasars are tracing peaks in the matter density field, then we would expect that on average the convergence will be enhanced in regions of high quasar density (and will be lower in regions of low density). This should be apparent in a "stack" of the convergence map at different positions of the density map. We define 10 density bins covering the range $-0.5 \leqslant \delta \leqslant 0.5$, split such that each bin represents the same sky area. The average κ for each bin is then

$$\bar{\kappa}|_\delta = \frac{1}{N}\sum_{i=0}^{N}\kappa(x_i, y_i) \tag{6}$$

where $\kappa(x_i, y_i)$ is the value of κ at the ith pixel in each δ bin. The significance of the stack can be estimated by repeating the procedure on an ensemble of 40 realistic noise simulations

[32] http://lambda.gsfc.nasa.gov/toolbox/tb_camb_form.cfm

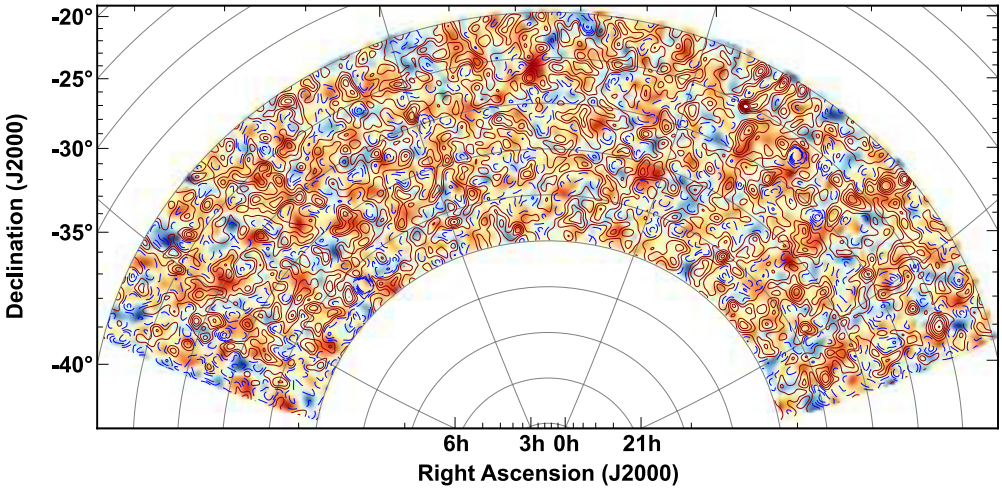

Figure 3. 2500 deg^2 SPT lensing convergence map with contours showing the fractional overdensity of quasars, both smoothed with a 1° Gaussian kernel. The color scale runs from blue→red for regions with negative to positive relative convergence (see Section 3). Contours span $-0.5 \leqslant \delta \leqslant 0.5$ in steps of $\delta = 0.1$; $\delta < 0$ contours are dashed. The CMB lensing convergence map and the quasar number density field are correlated at the 7σ level.

(A color version of this figure is available in the online journal.)

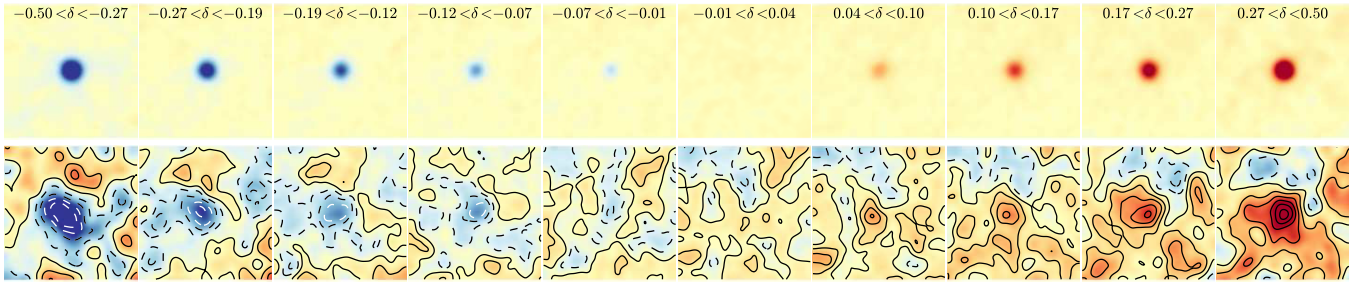

Figure 4. 5° thumbnail stacks showing (top) bins of fractional quasar density where we have stacked the δ map in bins spanning $-0.5 \leqslant \delta \leqslant 0.5$; (bottom) equivalent stacks evaluated at the same positions in the lensing convergence map. Contours show the significance in levels of 1σ, based on simulations (Section 2). Dashed contours indicate the significance in regions of $\kappa < 0$. A clear, significant transition from negative to positive CMB lensing convergence for lines of sight to low→high relative quasar density is evident, graphically illustrating the strong cross-correlation signal.

(A color version of this figure is available in the online journal.)

and taking the variance for each bin. Figure 4 presents the stacked images, showing a significant transition from mean negative convergence in regions of low quasar density to positive convergence in regions of high quasar density. This is clear evidence that *WISE*-selected quasars are tracing mass that is lensing the CMB.

4.1. Cross-power Spectrum

The cross-correlation is comprehensively measured through the cross-power spectrum (Equation (5)). Since the redshift distribution of the quasar population is reasonably well constrained (Section 2.2.2), this allows us to estimate the bias of the population. In Figure 5 we present the cross-power spectrum of the convergence map, M_κ, and quasar density map M_g:

$$C_l^{\kappa g} = \left\langle \mathrm{Re}(\mathcal{F}(\mathsf{M}_\kappa)\mathcal{F}^*(\mathsf{M}_\mathrm{g}))|_{\mathbf{l}\in l} \right\rangle \quad (7)$$

where $\mathbf{l} \in l$ describes the binning, such that the average power is calculated over all pixels in 2d Fourier space with coordinate $\mathbf{l}$ within the bin defined by l. As in Bleem et al. (2012), we mask bright stars identified by Two Micron All Sky Survey. When evaluating $C_l^{\kappa g}$ in bins of l, we correct for the transfer function described in Section 2.1, corresponding to a factor of ≈10%–30% for the bins shown.

Uncertainties are derived by repeating the calculation with 40 realistic noise simulations (Section 2.1) in place of the real

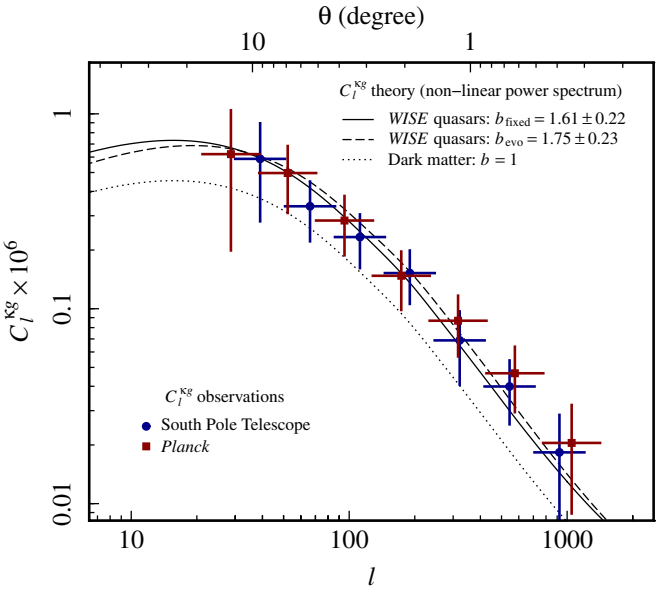

Figure 5. Cross-power spectrum of the *WISE*-selected quasar density and the CMB lensing convergence. The curves show (a) dark matter ($b = 1$, dotted), (b) the best-fit (to SPT) Equation (5), (solid), with constant bias and (c) evolving bias (dashed, Section 5).

(A color version of this figure is available in the online journal.)

convergence map and measuring the variance in $C_l^{\kappa g}$, where the mean correlation between the simulations and the quasar map is null for all l. Note that this procedure underestimates the sample variance contribution by a factor of $\sqrt{2}$, but since the quasar catalogue is shot-noise dominated, neglecting this will underestimate the uncertainty by less than 10%. Fitting Equation (5) for the bias, we find a best fit $b = 1.61 \pm 0.22$, with $\chi^2 = 1.32$ and $\chi^2/\nu = 0.26$. The significance is evaluated as the difference between the null line ($b = 0$) and the best fit theoretical spectrum: $\Delta\chi^2 = \chi^2_{\rm null} - \chi^2_{\rm fit}$, corresponding to a detection significance of 7.0σ. It is possible to obtain a more significant (13σ) signal if one simply cross-correlates a "generic extragalactic" sample defined by 15 mag $\leqslant W1 \leqslant$ 17 mag (e.g., Bleem et al. 2012), however, this population is so heterogeneous that it is difficult to interpret any derived parameters for the galaxies involved.

4.1.1. Planck Comparison

The availability of *Planck* data allows us to follow an identical procedure using an independent lensing map. An all-sky lensing potential map from *Planck* (Planck Collaboration XVII 2013a) retrieved from the Planck Legacy Archive is converted to lensing convergence using spherical harmonic transforms, then projected onto the SPT survey area. Figure 5 shows the excellent agreement between SPT and *Planck* cross-power spectra. Without realistic *Planck* simulations it is difficult to accurately estimate uncertainties, so the *Planck* error bars are derived from the l bin variance, which we have verified (using the SPT power spectrum) is a good estimate of the uncertainty derived from noise simulations. Generally, uncertainties in the *Planck* spectrum are ∼20% larger than SPT, however note that shot-noise in the quasar catalog is a significant contribution in the errors of both spectra. Furthermore, the strongly anisotropic noise in the lensing map (van Engelen et al. 2012) is not included in the cross-spectrum estimation, leading to sub-optimal power spectrum estimates, and therefore more similar error bars for *Planck* and SPT than might be naively expected.

5. INTERPRETATION

In ΛCDM, one can relate galaxy populations to dark matter halos of characteristic mass $M_{\rm h}$ (e.g., Peebles 1993), in the simplified case in which all objects in a given sample reside in halos of the same mass. $M_{\rm h}$ is related to the bias through the parameterization $b = f(\nu)$ where ν is the ratio of the critical threshold for spherical collapse to the rms density fluctuation for a mass M: $\nu = \delta_c/\sigma(M)$. Here we apply the fitting function of Tinker et al. (2010),[33] yielding $\log_{10}(M_{\rm h}/[h^{-1}M_\odot]) = 12.3^{+0.3}_{-0.2}$ for our measured $b = 1.61 \pm 0.22$, at $\langle z\rangle = 1.1$.

Sherwin et al. (2012) used galaxy–CMB lensing cross-correlation to measure the linear bias of SDSS photometrically-selected Type 1 quasars, finding $b = 2.5 \pm 0.6$ at $z \approx 1.5$. The bias of Type 1 quasars is observed to evolve over our redshift range (Croom et al. 2005; Ross et al. 2009), and indeed Sherwin et al. (2012) assume a fiducial model for $b(z)$ in their fit. The evolution of the bias of Type 1 and 2 quasars *combined* is not known; but if we assume a fiducial evolution model for $b(z)$ appropriate for Type 1, $b_{\rm evo} = 0.53 + 0.289(1+z)^2$ (Croom et al. 2005) and fit for the normalization of that model, $b = b_0 b_{\rm evo}$, we find $b_0 = 0.97 \pm 0.13$, corresponding to $b = 1.75 \pm 0.23$ at $\langle z\rangle = 1.1$ ($\log(M_{\rm h}/[h^{-1}M_\odot]) = 12.4^{+0.2}_{-0.3}$) (Figure 5). This is in excellent agreement with that of clustering analyses of Type 1 quasars ($b = 1.83 \pm 0.33$ at $z \approx 1$; Ross et al. 2009). Evolving this model for bias evolution to $z \approx 1.5$, we obtain $b = 2.27$, consistent with Sherwin et al. (2012).

The key difference between previous studies and ours is the fact that the *WISE* selection includes both Type 1 and Type 2 quasars. Due to the current paucity of deep optical data across the SPT footprint, we are unable to split our sample into Type 1 and 2 (Hickox et al. 2007). However, using our identical Boötes selection (Section 2.2.2), where a Type classification *can* be made (which is generally at $z > 0.7$), we find similar dn/dz, with $\langle z\rangle = 1.21$ and $\langle z\rangle = 1.11$ for Type 1 and 2 quasars (with similar mean bolometric luminosities of $\log(L_{\rm bol}/{\rm erg\,s^{-1}}) = 46.18$ and 46.16) respectively (Hickox et al. 2011). Assuming the similarity in the redshift distribution of Type 1 and 2 quasars persists to $z < 0.7$, then our result implies that Type 1 and 2 quasars trace the matter field in a similar way, given the similarity with the bias measured for Type 1 quasars alone.

The relative abundance of Type 1 and 2 quasars in our selection is ∼70:30, however, intrinsically they are thought to be approximately equally abundant (Ueda et al. 2003; Hopkins et al. 2007). This is explained through our bright cut in $W2$ (and strict $W1$–$W2$ selection), introducing incompleteness that preferentially affects the obscured quasars. The conclusions that follow make the assumptions that (1) Type 1 and 2 quasars are equally abundant and have similar redshift distributions, and (2) our bias measurement is representative of the population as a whole, at the bolometric luminosities sampled here.

6. CONCLUSIONS

Our result shows that the bias of a combined Type 1 and 2 quasar sample is consistent with that found for a Type 1 sample alone at $z \sim 1$. This is in agreement with Hickox et al. (2011), who conclude that Type 2 quasars must be at least as strongly clustered as Type 1 quasars. This is important for quasar evolution and unification schemes. In the unification model, Type 1 and 2 quasars are fundamentally the same population, but the geometry of the material obscuring the optically bright accretion disk results in an optical depth that is strongly dependent on viewing angle. In unification we would expect to find that the bias of a mixture of Type 1 and Type 2 quasars is the same as a Type 1-only sample selected from the same redshift distribution.

An alternative hypothesis is that obscured quasars become unobscured through a process that removes the optically thick nuclear screen (e.g., Hopkins et al. 2008). The relative bias of the populations can be related to the physics of the transitionary process. The similar bias parameters imply similar masses for the host halos, and therefore a comparable host halo number density. If the intrinsic abundances of obscured and unobscured quasars are roughly equal, and their bolometric luminosities similar, then this implies that the obscured and unobscured evolutionary phases must be of similar duration.

The technique of galaxy–CMB lensing cross-correlation is an exciting and powerful new tool for examining the complex relationship between luminous galaxies and the dark matter field they inhabit.

SPT is supported by the NSF through grants ANT-0638937 and ANT-0130612. Support for this work is provided by: the NSF Physics Frontier Center grant PHY-0114422 to the

[33] Assuming halos are all 200 times the mean density of the universe.

Kavli Institute of Cosmological Physics at the University of Chicago; the Kavli Foundation and the Gordon and Betty Moore Foundation; NSF (grant numbers 1211096, 1211112 and PHYS-1066293); NASA through ADAP award NNX12AE38G; NSERC, CIfAR, and the Canada Research Chairs program. This research used resources of the National Energy Research Scientific Computing Center, which is supported by the Office of Science of the U.S. DoE under contract DE-AC02-05CH11231. Research at Argonne National Laboratory is supported by the Office of Science of the U.S. DoE under contract DE-AC02-06CH11357. *Planck* is an ESA science mission with instruments and contributions directly funded by ESA Member States, NASA, and Canada.

REFERENCES

Abazajian, K., Adelman-McCarthy, J. K., Ageros, M. A., et al. 2009, ApJS, 182, 543
Assef, R. J., Stern, D., Kochanek, C. S., et al. 2013, ApJ, 772, 26
Bleem, L. E., van Engelen, A., Holder, G. P., et al. 2012, ApJL, 753, L9
Brodwin, M. J. I., Brown, M. J. I., Ashby, M. L. N., et al. 2006, ApJ, 651, 791
Carlstrom, J. E., Ade, P. A. R., Aird, K. A., et al. 2011, PASP, 123, 568
Cooray, A., & Hu, W. 2000, ApJ, 534, 533
Croom, C. M., Boyle, B. J., Shanks, T., et al. 2005, MNRAS, 356, 415
Das, S., Sherwin, B. D., Aguirre, P., et al. 2011, PhRvL, 107, 021301
Hickox, R. C., Jones, C., Forman, W. R., et al. 2007, ApJ, 671, 1365
Hickox, R. C., Myers, A. D., Brodwin, M., et al. 2011, ApJ, 731, 117
Hirata, C. M., Ho, S., Padmanabhan, N., Seljak, U., & Bahcall, N. A. 2008, PhRvD, 78, 043520
Holder, G. P., Viero, M. P., Zahn, O., et al. 2013, ApJL, 771, L16
Hopkins, P. F., Hernquist, L., Cox, T. J., & Keres, D. 2008, ApJS, 175, 356
Hopkins, P. F., Richards, G. T., & Hernquist, L. 2007, ApJ, 654, 731
Hu, W. 2001, ApJL, 557, L79
Kaiser, N. 1992, ApJ, 388, 272
Kochanek, C. S., Eisenstein, D. J., Cool, R. J., et al. 2012, ApJS, 200, 8
Komatsu, E., Smith, K. M., Dunkley, J., et al. 2011, ApJS, 192, 18
Lacy, M., Storrie-Lombardi, L. J., Sajina, A., et al. 2004, ApJS, 154, 166
Lewis, A., Challinor, A., & Lasenby, A. 2000, ApJ, 538, 473
Limber, D. N. 1953, ApJ, 117, 134
Peebles, P. J. E. 1993, Principles of Physical Cosmology (Princeton, NJ: Princeton Univ. Press)
Planck Collaboration XVII. 2013a, arXiv:1303.5077
Planck Collaboration XVIII. 2013b, arXiv:1303.5078
Polletta, M., Tajer, M., Maraschi, L., et al. 2007, ApJ, 663, 81
Ross, N. P., Shen, Y., Strauss, M. A., et al. 2009, ApJ, 697, 1634
Seljak, U., & Zaldarriaga, M. 1999, PhRvL, 82, 2636
Sherwin, B. D., Das, S., Hajian, A., et al. 2012, PhRvD, 86, 083006
Smith, K. M., Zahn, O., & Doré, O. 2007, PhRvD, 76, 043510
Smith, R. E., Peacock, J. A., Jenkins, A., et al. 2003, MNRAS, 341, 1311
Song, Y.-S., Cooray, A., Knox, L., & Zaldarriaga, M. 2003, ApJ, 590, 664
Stern, D., Eisenhardt, P., Gorjian, V., et al. 2005, ApJ, 631, 163
Story, K. T., Reichardt, C. L., Hou, Z., et al. 2012, arXiv:1210.7231
Tinker, J. L., Robertson, B. E., Kravtsov, A. V., et al. 2010, ApJ, 724, 878
Ueda, Y., Akiyama, M., Ohta, K., & Miyaji, T. 2003, ApJ, 598, 886
van Engelen, A., Keisler, R., Zahn, O., et al. 2012, ApJ, 756, 142
Vega, O., Clemens, M. S., Bressan, A., et al. 2008, A&A, 484, 631
Wright, E. L., Eisenhardt, P. R. M., Mainzer, A. K., et al. 2010, AJ, 140, 1868
Yan, L., Donoso, E., Tsai, C.-W., et al. 2013, AJ, 145, 55